ACS APPLIED MATERIALS & INTERFACES

www.acsami.org

Research Article

EDTA-Inspired Polydentate Hydrogels with Exceptionally High Heavy Metal Adsorption Capacity as Reusable Adsorbents for Wastewater Purification

Sudipta Panja,* Samuel Hanson, and Chun Wang*

Cite This: *ACS Appl. Mater. Interfaces* 2020, 12, 25276−25285

Read Online

ACCESS | Metrics & More | Article Recommendations | Supporting Information

ABSTRACT: Water pollution by heavy metal ions is a critical threat to public health. To remove the heavy metal pollutants from large waterbodies, we have synthesized a biocompatible, cost-effective, metal ion non-specific, and ethylenediaminetetraacetic acid (EDTA)-inspired polydentate hydrogel with exceptionally high adsorption capacity and reusability. The hydrogel was synthesized by the transamidation reaction between hydrolyzed polyacrylamide and branched polyethylenimine (BPEI). The mechanical strength of the synthesized hydrogel displayed an increasing trend with the wt % of the cross-linker (BPEI) and achieved a maximum storage modulus (G'_{max}) of 1093 Pa. Scanning electron microscopy revealed a porous network structure of the hydrogel (pore size: 30−70 μm), resulting in a very high swelling ratio of 5800%. The porous hydrogel manifested the maximum adsorption capacity of 482.2 mg/g when adsorbing from a mixture of metal ions (Cr^{3+}, Cu^{2+}, Zn^{2+}, Cd^{2+}, Hg^{2+}, and Pb^{2+}), higher than any EDTA-grafted material known to date. The high adsorption capacity of the hydrogel was attributed to the existence of numerous EDTA-mimicking coordinating functional groups, as confirmed by X-ray photoelectron spectroscopy. In addition, the hydrogel showed the self-healing property and preserved more than 85% adsorption efficiency even after five cycles of reuse. Furthermore, the hydrogels showed no or moderate toxicity toward mammalian cells.

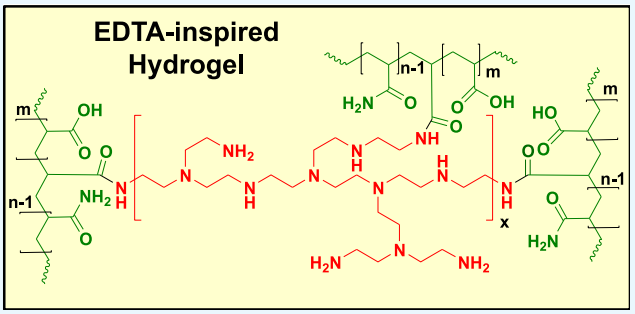

KEYWORDS: *Hydrogel, multidentate ligand, metal ion adsorbent, water purification, EDTA*

1. INTRODUCTION

Water pollution by heavy metal contamination is one of the critical threats to the environment, living organisms, and public health.[1−3] Over the last few decades, various biological, chemical, and physical separation techniques for heavy metal removal have been developed, including nanofiltration, solvent extraction, electrodialysis, membrane separation, ion exchange, and adsorption processes.[3] Adsorption is considered a superior technique because of the simplicity of the treatment, cost-effectiveness, efficiency for purification, and absence of secondary pollution.[4] The adsorption of heavy metal ions has been achieved by employing various materials such as bio-organism-derived biosorbents,[5] ligand-functionalized porous polymeric materials,[6] and metal−organic frameworks (MOFs).[7,8] However, the materials currently available are not ideal, because of their limited adsorption capacity toward a broad spectrum of heavy metal ionic species,[9] tedious process of separation from wastewater, and lack of reusability.

Polymeric hydrogels with a three-dimensional cross-linked network structure and appropriate functional groups[10] may be ideal heavy metal ion adsorbents with potential for achieving high binding capacity,[11] mechanical integrity, and reusability. Hydrogels based on a variety of natural and synthetic homopolymers/copolymers, such as chitosan,[5] cellulose,[1] carboxymethyl cellulose (CMC),[12] CMC-*grafted*-poly(*N*-isopropyl acrylamide-*co*-acrylic acid),[13] crown ether derivative of polystyrene,[14] and poly(acrylamide-*co*-4-vinyl pyridine),[15] have been evaluated for scavenging heavy metal ions. These polymeric structures share some common functional groups, including hydroxyl (−OH), thiol (−SH), carboxyl (−COO−), and amines ($-NH_2$, −RNH−, and $-R_2N$), which are responsible for the binding of heavy metal ions.[12] In contrast to single metal-binding functional groups, polydentate ligands are highly efficient nonspecific chelators. For example, ethylenediaminetetraacetic acid (EDTA) has four hard "−COOH" and two relatively soft "$-NR_2$" coordinating sites for binding a wide range of heavy metal ions.[9] However, metal chelates formed by EDTA are soluble in water, and hence are

Received: February 26, 2020
Accepted: May 8, 2020
Published: May 8, 2020

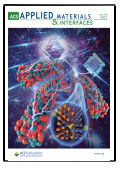

https://dx.doi.org/10.1021/acsami.0c03689
ACS Appl. Mater. Interfaces 2020, 12, 25276−25285

Scheme 1. Synthesis of EDTA-Inspired Polydentate Hydrogels through the Transamidation Reaction between Partially HPAM and BPEI. The Mixture of HPAM and BPEI before and after Gelation are Shown in the Right Panel

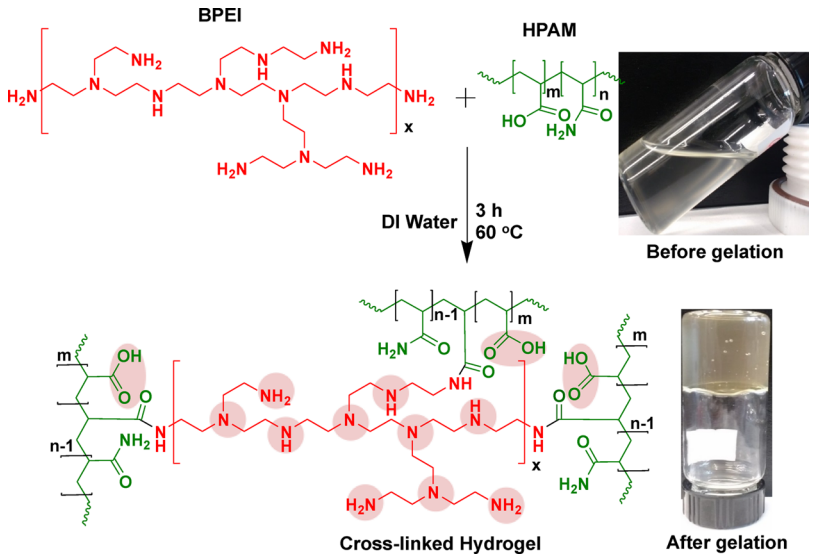

difficult to be separated from large polluted waterbodies. Recently, several attempts have been made to incorporate EDTA into the existing adsorbent systems to achieve enhanced adsorption capacity.[5,9] Examples include EDTA-modified *N*,*N*-methylene bis(acrylamide)-cross-linked polyacrylamide hydrogels,[5] EDTA-grafted MOFs,[9] EDTA-cross-linked covalent organic frameworks,[16] EDTA-modified bacterial cellulose membranes,[17] and EDTA-grafted magnetic nanoparticles.[18] However, covalent grafting and cross-linking approaches of EDTA through one or two of the carboxylic acid groups is not easy and reduces the number of active functional groups available for metal chelation. It is also difficult to achieve a high grafting density for EDTA because the neighboring carboxylic acid groups pose steric and electrostatic hindrance. In this context, we set out to design EDTA-inspired polydentate hydrogels containing the same metal-chelating functional groups as in EDTA, but not requiring EDTA grafting. Such a hydrogel could be synthesized through a one-pot reaction between a suitably functionalized linear polymer and a cross-linker while preserving all the active metal-chelating groups, potentially achieving exceptionally high heavy metal adsorption capacity.

Here, we report the one-step synthesis of EDTA-inspired polydentate hydrogels from partially hydrolyzed polyacrylamide (HPAM)[19] and branched polyethylenimine (BPEI). HPAM, as a functional polymer precursor, is cross-linked with BPEI via a transamidation reaction[20−22] between the primary amines ($-NH_2$) of BPEI and the amide groups ($-CONH_2$) of HPAM side chains, resulting in the formation of renewed amide ($-CONH-$) linkages. These hydrogels contain numerous hard "−COOH" groups in the side chains of HPAM and relatively soft secondary ($-NH-$) and tertiary ($-NR_2$) amine groups in BPEI, and are expected to form chelates with a wide range of heavy metal ions in a manner similar to EDTA. The chemical structure, surface composition, microstructure, and mechanical properties of the synthesized hydrogels were characterized. Their adsorption capacity of heavy metal ions commonly found in polluted water was determined under single-component and multiple-component conditions and compared with state-of-the-art materials reported in the literature. Additional useful features of hydrogels for wastewater purification, including self-healing and regeneration of metal-scavenging capacity after multiple cycles, were also examined.

2. EXPERIMENTAL SECTION

2.1. Materials. Partially HPAM or poly(acrylamide-*co*-acrylic acid) (M_n = 150 kDa, acrylic acid content: 20 wt %) and BPEI (M_n = 0.6 kDa) were purchased from Sigma-Aldrich, USA. Zinc chloride ($ZnCl_2$), copper sulfate pentahydrate ($CuSO_4{\cdot}5H_2O$), mercuric chloride ($HgCl_2$), cadmium chloride ($CdCl_2$), chromium trioxide (CrO_3), and lead nitrate ($Pb(NO_3)_2$) were purchased from Fisher Scientific, USA. DMEM cell culture media, fetal bovine serum (FBS), penicillin, streptomycin, live-cell imaging solution (LCIS), and NucBlue Live ReadyProbes Reagent (Hoechst 33342) were all purchased from Thermo-Fisher Scientific, USA. All other chemicals including solvents were purchased from Sigma and used without further purification.

2.2. Further Hydrolysis of HPAM and Determination of the Degree of Hydrolysis by Acid−Base Titration. HPAM with 20 wt % degree of hydrolysis was hydrolyzed further to produce 50 wt % HPAM by base-catalyzed hydrolysis, as reported by Zeynali et al.[23] In brief, 100 mL of 5 wt % solution of HPAM (20 wt % hydrolyzed) was taken in a round bottom flask followed by the addition of 10 mL of NaOH solution (0.2 g/mL). The flask was then placed in an oil bath preheated to 60 °C. After a particular time period (e.g., 2, 4, and 8 h), a small aliquot was removed from the reaction mixture and acidified to pH 3 (corresponding to the pK_a of "−COOH") with 0.1 N HCl. The acidified solution was back titrated with 0.1 N standard solution of NaOH to neutral pH 7. The equivalent of NaOH consumed to bring a given amount of HPAM solution from pH 3 to pH 7 is proportional to the equivalent of "−COOH" present in the given HPAM solution. The hydrolysis reaction was stopped after reaching ∼50 wt % hydrolysis (approximately after 8 h). The reaction mixture was then cooled down to room temperature and precipitated in cooled methanol. The precipitated polymer was dried under vacuum at 80 °C.

2.3. Hydrogel Synthesis. The hydrogels were synthesized by the transamidation reaction between the amide group of HPAM and the amine group of BPEI (Scheme 1). HPAM powder (1 g) was dissolved in 10 mL of DI water followed by mixing with various amounts of BPEI (1, 3, 5, 10, and 20 wt % with respect to HPAM). The initial pH of the HPAM solution was pH 5.5 and it increased to pH 8 after the addition of BPEI. The mixed solution was then transferred to a glass

https://dx.doi.org/10.1021/acsami.0c03689
ACS Appl. Mater. Interfaces 2020, 12, 25276−25285

vial, sealed with a septum, placed in a preheated oil bath of 60 °C, and allowed to react for 3 h. A needle was passed through the septum to remove the ammonia gas produced from the reaction. The synthesized hydrogel was cooled down to room temperature and immersed in 1 L of deionized water overnight to remove any unreacted reagents. The swollen hydrogel was then lyophilized.

2.4. Physicochemical Characterization of Hydrogels. The ^{1}H NMR spectra were recorded at 400 MHz using a Bruker AVANCE III spectrometer. Samples were dissolved in DMSO-d_6. The attenuated total reflection−Fourier transform infrared (ATR−FTIR) spectra of the hydrogel were recorded on a Bruker ALPHA PLATINUM spectrometer equipped with a diamond crystal attachment. High-resolution X-ray photoelectron spectra of the dried hydrogel powder were recorded using an "Al" Kα X-ray (photon energy: 1486.7 eV) source. Data analysis was performed on CasaXPS processing software. The surface morphology of the hydrogels was captured using a Hitachi S-5500 scanning electron microscope. Samples were mounted on a carbon tape-coated scanning electron microscope sample holder and sputtered with gold to capture the surface morphology.

2.5. Hydrogel Swelling and Rheological Characterization. Samples of dried hydrogels were weighed and immersed in excess amount of DI water for 24 h. After removing surface water, the wet gels were weighed again. The swelling ratio in % was calculated as: $(W_s - W_d)/W_d \times 100\%$, where W_d is the weight of the dried gel and W_s is the weight of the wet gel at equilibrium.

The mechanical integrity of the hydrogels was evaluated based on their frequency-dependent rheological behavior. The gel sample was placed between the two parallel plates of the rheometer (AR-G2 model) and the gap between the plates was maintained at 1 mm. The frequency sweep experiment was performed at 25 °C with a constant strain of 1% and a frequency range from 0.01 to 100 Hz.

2.6. Metal Ion Adsorption Isotherm. The adsorption isotherm of the hydrogel was determined by incubating 5 mg of the dried hydrogel in 50 mL of various concentrations (5−500 ppm) of metal ions. The experiment was performed with three different metal ions, Cr^{3+} (hard), Cu^{2+} (borderline), and Hg^{2+} (soft), over 24 h under continuous shaking at RT. After the allotted time, the solution was filtered through a 0.2 μm nylon syringe filter. The concentration of metal ions present in the filtrate was determined using an Agilent 700 Series inductively coupled plasma-optical emission spectrometer and 2% HNO_3 solution as a carrier. The filtrate's concentration was subtracted from the feed concentration to get the actual value of metal ions adsorbed by the hydrogel for a particular concentration. The adsorption isotherm was fit with the Langmuir (eq 1) and Freundlich (eq 2) adsorption models.[9] A linear correlation coefficient was obtained after linear fitting.

Langmuir adsorption isotherm

$$\frac{C_e}{q_e} = \frac{1}{q_m K_L} + \frac{C_e}{q_m} \tag{1}$$

where q_e (mg/g) is the amount of metal ions adsorbed by the hydrogel, representing the maximum adsorption capacity for the monolayer, C_e (ppm) is the metal ion concentration at equilibrium, and K_L is the Langmuir constant.

Freundlich adsorption isotherm

$$\ln q_e = \ln K_F + \frac{1}{n} \ln C_e \tag{2}$$

where q_e (mg/g) is the amount of metal ions adsorbed by the hydrogel; C_e (ppm) is the metal ion concentration at equilibrium; n and K_F represent the Freundlich constants associated with adsorption intensity and adsorption capacity, respectively.

2.7. Metal Ion Adsorption Kinetics. To determine the metal ion adsorption kinetics, 5 mg of dried hydrogel was added to 50 mL of 50 ppm stock solution (in deionized water) of different heavy metal ions (Cr^{3+}, Cu^{2+}, Zn^{2+}, Cd^{2+}, Hg^{2+}, and Pb^{2+}) under continuous shaking at RT. After each short interval of time, an aliquot was removed from the solution and filtered through a 0.2 μm nylon syringe filter. The adsorption capacity of the hydrogel at each time point was determined by inductively coupled plasma-optical emission spectrometry (ICP-OES) as mentioned earlier. The experimental results were fit with pseudo-first-order (eq 3) and pseudo-second-order kinetic models (eq 4).[9]

Pseudo-first-order kinetics

$$\ln(q_e - q_t) = \ln q_e - K_1 t \tag{3}$$

where q_t represents the adsorption capacity at time t, q_e represents the equilibrium adsorption capacity, and K_1 represents the pseudo-first-order rate constant.

Pseudo-second-order kinetics

$$\frac{t}{q_t} = \frac{t}{q_e} + \frac{1}{K_2 q_e^2} \tag{4}$$

where qt represents the adsorption capacity at time t, q_e represents the equilibrium adsorption capacity, and K_2 represents the pseudo-second-order rate constant.

2.8. Determination of Adsorption Capacity. To determine the equilibrium adsorption capacity for heavy metal ions, 5 mg of the dried hydrogel was added to 50 mL of 50 ppm stock solution of six different heavy metal ions (Cr^{3+}, Cu^{2+}, Zn^{2+}, Cd^{2+}, Hg^{2+}, and Pb^{2+}) with continuous shaking over 24 h. The adsorption capacity was determined by ICP-OES and expressed as mg of metal/g of the dry hydrogel. The experiment was conducted under both single-component (one type of metal ion at a time) and multiple-component (all six metal ions combined, each at 50 ppm) conditions.

2.9. Reusability of Hydrogels. First, dried hydrogels were equilibrated in single metal ion solutions and the amount of adsorbed ions was determined as described above. To remove the metal ions, the hydrogels were stirred in a 5% (v/v) HNO_3 aqueous solution for 24 h. The hydrogels were then separated from the HNO_3 solution and washed three times with Milli-Q water. Next, the hydrogels were lyophilized for the next cycle of ion adsorption and removal. Five consecutive cycles were completed and the metal ion adsorption efficiency after each cycle was measured.

2.10. Visual Inspection of Hydrogel Swelling, Metal Ion Adsorption, and Self-Healing. Hydrogels were photographed under the following conditions: (1) fully dried, (2) fully swollen in water, and (3) after incubation in 50 ppm Cu^{2+} solution. To demonstrate self-healing behavior, a circular hydrogel disc was cut into two halves. One half was stained with rhodamine B (red) and the other half with methylene blue (blue). The two pieces of the hydrogel were then brought in contact with their cut surfaces aligned for 6 h at room temperature.

2.11. Cell Viability Assay. Mouse fibroblast cells (NIH/3T3, ATCC CRL-1658) were grown in DMEM-high glucose medium supplemented with 10% heat-inactivated FBS, penicillin (100 U/mL), and streptomycin (100 μg/mL). Cells were grown in 75 cm^2 polystyrene tissue culture flasks and incubated at 37 °C, 5% CO_2, and 95% relative humidity. They were plated at 10,000 cells/well (in 200 μL of phenol red-free medium) in a 48-well plate. After culturing for 24 h, the medium was removed and 200 μL of medium containing various concentrations (50, 100, 500, and 1000 μg/mL) of dry hydrogel powder was added to the cells. After 24 h of exposure, the medium of each well was replaced with 200 μL of fresh phenol red-free medium. Cell viability was measured using an MTT assay.[24] To each well, 20 μL of MTT solution (12 mM in PBS) was added. After 4 h, 170 μL was removed from each well and formazan was solubilized in 200 μL of dimethyl sulfoxide (DMSO). Absorbance was measured at 540 nm using a plate reader (BioTek Cytation 3 Cell Imaging Multi-Mode Reader controlled by Gen5 all-in-one microplate reader software).

2.12. Cell Morphology Study. NIH/3T3 cells were plated at 50,000 cells/well (in 1 mL of phenol red-free medium) in a 12-well plate. After culturing for 24 h, the medium was removed and 1 mL of medium containing various concentrations of dry hydrogel powder was added to the cells. After 24 h of exposure, the medium was replaced by 1 mL of LCIS added to each well. Cell nuclei were stained by adding two drops of NucBlue Live ReadyProbes Reagent (Hoechst

https://dx.doi.org/10.1021/acsami.0c03689
ACS Appl. Mater. Interfaces 2020, 12, 25276−25285

33342), followed by 20 min of incubation. Phase-contrast images of cells were captured with an Olympus IX70 inverted system microscope equipped with an Olympus DP72 microscope digital camera and a 10× (0.25 NA) objective with an additional 1.5× auxiliary lens. Cells were imaged with phase contrast and stained nuclei were imaged with a DAPI/Hoechst/AMCA filter (λ_{ex} = 350/50 nm, λ_{em} = 460/50 nm).

3. RESULTS AND DISCUSSION

3.1. Synthesis of Hydrogel and Characterization by NMR, FTIR, and XPS. The EDTA-inspired polydentate hydrogels were synthesized by the transamidation reaction[21] between two polyelectrolytes, HPAM and BPEI. The transamidation involved the reaction between the amine group (-NH_2) of BPEI and the amide group (-$CONH_2$) of HPAM. The aqueous solution of HPAM (10 wt %) was mixed with different wt % of BPEI and placed in an oil bath at 60 °C for 3 h to synthesize the hydrogel (Scheme 1). The HPAM solution turned into gel with the release of NH_3 gas. Here, we have reported four different types of hydrogels using 20 and 50 wt % acrylic acid containing HPAM and two different wt % of BPEI. The detailed compositions of the hydrogels (HG-1−4) are provided in Table 1. HG-1 and HG-2 gels were synthesized from 50 wt % acrylic acid containing HPAM with 10 and 20 wt % BPEI, respectively. HG-3 and HG-4 gels were synthesized from 20 wt % acrylic acid containing HPAM with 10 and 20 wt % BPEI, respectively. The hydrogels were then characterized by ATR−FTIR and the spectra are displayed in Figure S1. Pristine HPAM (50 wt % acrylic acid content) showed absorbance bands at 3415, 3210, and 2944 cm^{-1}, which were assigned to bond stretching corresponding to "−N−H", "−O−H", and "−C−H", respectively. The stretching band at 1665 cm^{-1} was assigned to the "−C═O" stretching frequency of both "−COOH" and "−$CONH_2$". Conventionally, the "−C═O" stretching frequency of "−COOH" should appear at 1710 cm^{-1};[25,26] however, the intermolecular hydrogen bonding interaction reduced the stretching frequency to a somewhat lower wavenumber, which merged with the "−C═O" stretching frequency of "−$CONH_2$". Notably, after the formation of the hydrogel, the "−C═O" stretching band maxima of "−$CONH_2$" slightly shifted to a higher wavenumber (i.e. from 1665 to 1680 cm^{-1}). The shifting of the "−C═O" absorbance band to a higher wavenumber was ascribed to the transformation of "−$CONH_2$" to "−CONH−BPEI" through the transamidation reaction (Scheme 1). Furthermore, the ^{1}H NMR spectra (Figure S2b) of HPAM displayed signals at 7.22 and 6.80 ppm, which were assigned to the amide protons (−CON$\underline{\mathbf{H}}_2$; e). The signals at 2.07 and 1.45 ppm were attributed to the methyne (−C$\underline{\mathbf{H}}$−; d) and methylene (−C$\underline{\mathbf{H}}_2$−; c) protons of the backbone of HPAM. Importantly, the ^{1}H NMR spectrum of the hydrogel (Figure S2c) displayed a new peak at 7.77 ppm, which was not present in BPEI (Figure S2a) or HPAM (Figure S2b). This signal was attributed to the HPAM's amide proton (−CON$\underline{\mathbf{H}}$(BPEI); f) as the result of cross-linking with BPEI.

Table 1. Composition and Properties of EDTA-Inspired Polydentate Hydrogels[a]

sample	HPAM acrylic acid content (wt %)	BPEI (wt %)	[b] G'_{max} (Pa)	[c] τ_{crit} (s)	[d] swelling ratio (wt/wt, %)
HG-1	50	10	341	0.044	5846 ± 58.2
HG-2	50	20	1093	0.026	2732 ± 37.8
HG-3	20	10	326	0.051	4356 ± 48.5
HG-4	20	20	985	0.023	2132 ± 31.6

[a]All the gel samples were synthesized from 10 wt % stock solution of HPAM in water. [b]The maximum storage modulus was obtained from rheology. [c]Critical relaxation time was calculated from the reciprocal of the critical frequency obtained at the crossover point. [d]Swelling ratio (wt/wt) was obtained at equilibrium swelling (as mentioned in the Experimental Section).

Chemical changes to HPAM (polymer precursor) and BPEI (cross-linker) as a result of hydrogel formation were further characterized by high-resolution XPS spectroscopy (HR-XPS). The HR-XPS spectra of C 1s for both HPAM (Figure 1a) and the hydrogel (Figure 1b) displayed three comparable peaks at 285.9, 287.4, and 289 eV, which were assigned to the "C−C" backbone, "−COOH", and "−$CONH_2$" functional groups, respectively. The O 1s HR-XPS spectrum of HPAM (Figure 1c) displayed peaks at 528.8 and 530.2 eV, which were attributed to "−$CONH_2$" and "−COOH", respectively. The O 1s peaks of the hydrogel (Figure 1d) corresponding to "−$CONH_2$" and "−COOH" also appeared with the same binding energy as HPAM. This observation demonstrated the absence of any significant interaction between "−COOH" of HPAM and BPEI, meaning that the COOH groups of HPAM were fully intact after the cross-linking reaction and readily available for metal ion binding. Furthermore, the N 1s HR-XPS spectrum of HPAM (Figure 1e) showed a single peak at 397.2 eV, which was assigned to "−$CONH_2$" of the polymer. Meanwhile, the N 1s spectrum of the hydrogel (Figure 1f) showed an additional peak at 398.6 eV along with the existing peak at 397.2 eV. This additional peak at a higher binding energy (398.6 eV) was assigned to "−CONH (BPEI)", formed by the transamidation reaction between the "−NH_2" group of BPEI and the "−$CONH_2$" group of HPAM as shown in Scheme 1. These observations confirmed the success of the transamidation reaction-mediated hydrogel formation of HPAM and BPEI and the presence of key functional groups for metal ion chelation.

3.2. Hydrogel Morphology, Rheology, and Degree of Swelling. A series of hydrogels were synthesized with increasing percentage of the cross-linker (BPEI) as mentioned in the Experimental Section. The surface morphology and the microstructure of hydrogels were captured by scanning electron microscopy (SEM) after lyophilization. As the BPEI content increased from 1 to 5 wt %, the grain size of molecular aggregates seen in the SEM images increased, but the amount of BPEI cross-linker was not sufficient to form hydrogels (Figures 2a−4c). At 10 wt % of BPEI, the polymers displayed a continuous porous network structure with an average pore size of 70 μm (Figure 2d). A further increase of the BPEI content to 20 wt % led to a higher cross-linker density and reduced the pore size to an average value of 30 μm (Figure 2e). A magnified SEM image of the porous structure of the hydrogel with 20% BPEI is shown in Figure 2f. The porous architecture might allow a large influx of wastewater containing heavy metal ions and enhance the scavenging capacity of the hydrogel.

The rheological property of the synthesized hydrogel was tested under the frequency-dependent oscillation mode. The frequency-dependent variation of storage (G') and loss modulus (G'') is displayed in Figure 3. The storage modulus G' for all the synthesized hydrogels was higher than their corresponding loss modulus component G'', which validates the successful synthesis of the elastic network. Hydrogel with 20 wt % BPEI (sample HG-2, Table 1, Figure 3b) displayed

https://dx.doi.org/10.1021/acsami.0c03689
ACS Appl. Mater. Interfaces 2020, 12, 25276−25285

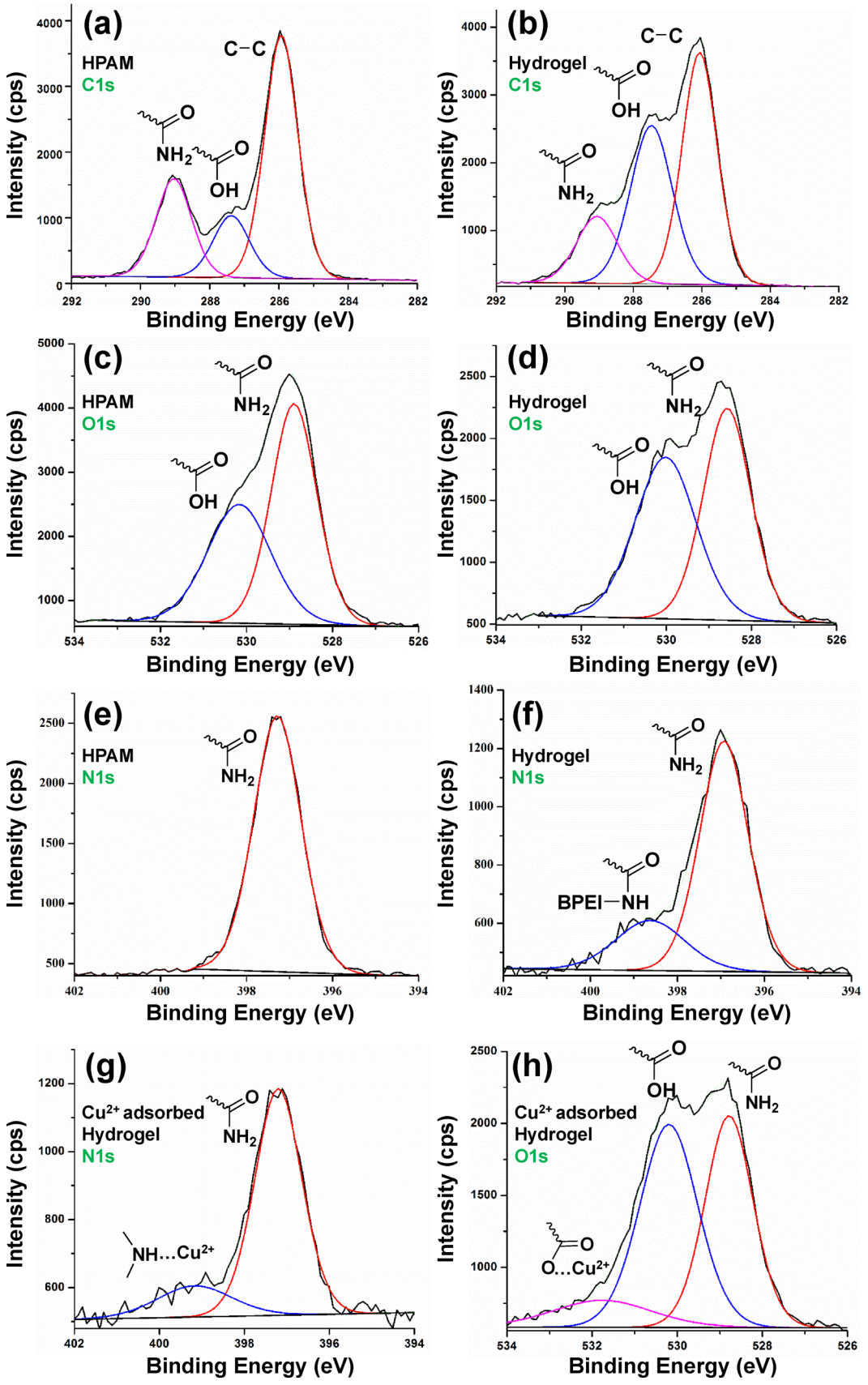

Figure 1. HR-XPS spectra of HPAM and EDTA-inspired polydentate hydrogels before and after metal chelation. (a) C 1s, HPAM. (b) C 1s, hydrogel. (c) O 1s, HPAM. (d) O 1s, hydrogel. (e) N 1s, HPAM. (f) N 1s, hydrogel. (g) N 1s, Cu^{2+} adsorbed gel. (h) N 1s, Cu^{2+} adsorbed gel.

https://dx.doi.org/10.1021/acsami.0c03689
ACS Appl. Mater. Interfaces 2020, 12, 25276−25285

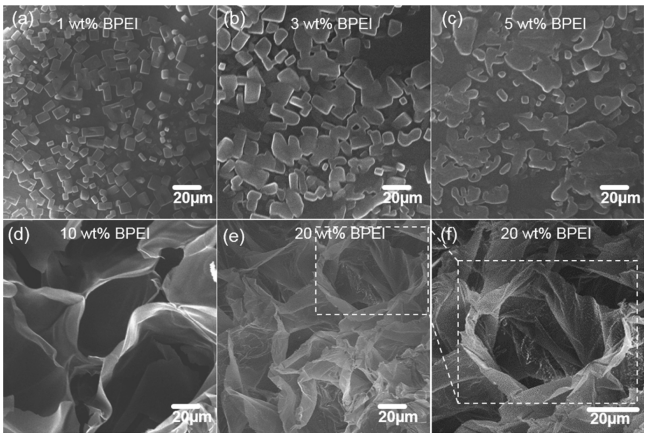

Figure 2. SEM images of HPAM polymer (acrylic content: 50 wt %) with increasing wt % of the cross-linker BPEI from (a) 1 to (b) 3 to (c) 5 wt %. SEM images of the hydrogel with 10 (d, sample HG-1) and 20 wt % (e, sample HG-2) of BPEI. Magnified SEM images of the hydrogel with 20 wt % cross-linker (f, sample HG-2).

G'_{max} = 1093 Pa, which was higher than the hydrogel prepared with 10 wt % BPEI (G'_{max} = 341 Pa, HG-1, Figure 3a). Hence, the hydrogel with a higher percentage of BPEI (20 wt %, HG-2) was stronger because of the higher cross-linker density. With increasing frequency, G' started to decrease, and finally, the G' and G'' crossed over each other. The frequency corresponding to the crossover point is known as the critical frequency.[10] Hence, beyond the critical frequency, the hydrogel network was disrupted and it started to flow. The reciprocal of the critical frequency was defined as the critical relaxation time (τ_{crit}). The τ_{crit} of the stronger hydrogel, HG-2, was 0.026 s and the weaker hydrogel, HG-1, was 0.044 s. The shorter τ_{crit} of HG-2 gel indicates that under dynamic stress the more densely cross-linked gel was able to recover its interconnected network more quickly than the less densely cross-linked HG-1 gel. These results demonstrate that the hydrogels with an interconnecting network structure have robust mechanical integrity, which would allow easy handling and separation from large waterbodies after metal ion adsorption.

The swelling behavior of the synthesized hydrogels was determined after the hydrogels reached their equilibrium swelling. The equilibrium swelling ratio (wt/wt) of the

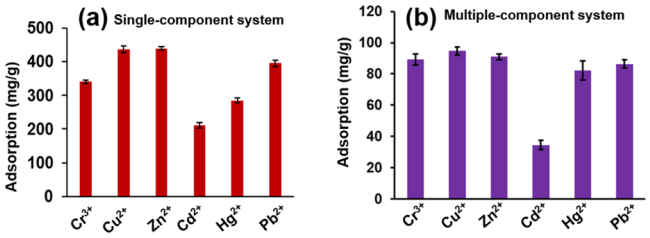

Figure 4. Equilibrium adsorption capacities of metal ions tested in (a) a single-component system and (b) multiple-component systems over a period of 24 h at room temperature.

synthesized hydrogels, HG-1−4, was determined as 5846, 2732, 4356, and 2132%, respectively. Representative images of the dry and swelled hydrogels are displayed in Figure S3a,b. HG-1 gel had a higher swelling ratio than HG-2, which was attributed to the different amounts of cross-linker (10 wt % for HG-1 compared to 20% for HG-2). Interestingly, the swelling ratio of HG-1 gel was much higher than HG-3, although both had an equal percentage of cross-linker (10 wt %). This could be explained by the fact that HG-1 was synthesized from 50 wt % acrylic acid containing HPAM and had higher numbers of hydrophilic "−COOH" groups than HG-3 gel (synthesized from 20 wt % acrylic acid containing HPAM). Hence, HG-1 gel with a high swelling ratio would be a preferred material capable of absorbing a huge proportion of water along with its dissolved heavy metal ions.

We further demonstrated that the synthesized hydrogels showed self-healing property. To demonstrate self-healing, a circular hydrogel disk was cut into two halves and separately stained with two different dyes (red and blue). Two pieces of the stained hydrogel were bought in contact at their cut edge surface. The two parts of the hydrogel healed to become a single piece after 6 h at room temperature (Figure S3c). The self-healing property could be well understood by recognizing the mechanism of gel formation and intermolecular hydrogen bonding interaction of the existing functional groups. The HPAM hydrogel was formed by covalent bonding between "−$CONH_2$" of HPAM and "−NH_2" of BPEI, leaving the "−COOH" group (of HPAM) intact (Scheme 1). We hypothesized that the remaining "−COOH" groups might be involved in hydrogen bonding with the remaining "−NH_2" and "−NH−" groups of BPEI along with the intermolecular hydrogen bonding interaction among the "−COOH" groups of

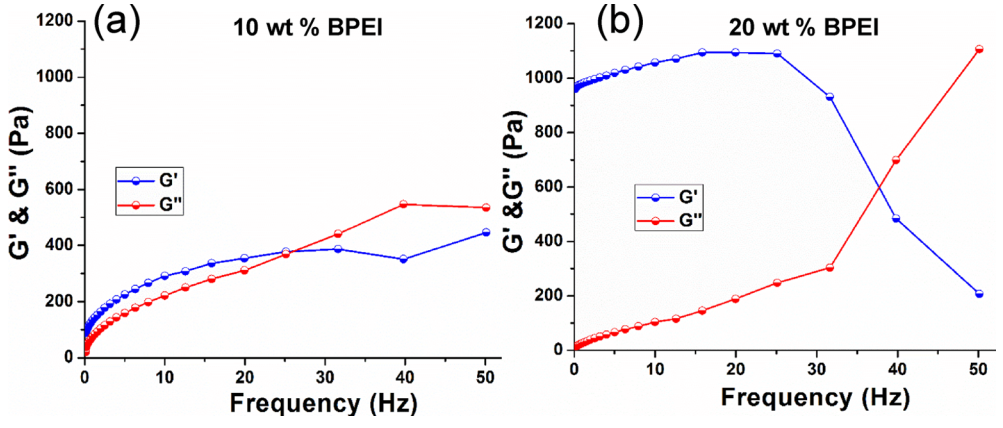

Figure 3. Rheological behavior of hydrogels consisting of HPAM cross-linked with (a) 10 wt % (sample HG-1) and (b) 20 wt % (sample HG-2) BPEI.

https://dx.doi.org/10.1021/acsami.0c03689
ACS Appl. Mater. Interfaces 2020, 12, 25276−25285

HPAM. The reversible hydrogen bonding interaction and the dynamic covalent transamidation reaction[27] might favor the reconstruction of the network between the two separate pieces of the hydrogel followed by healing into a single piece (Figure S1c). The self-healing behavior allowed small pieces of hydrogel to fuse into a large piece after metal ion scavenging (Figure S3d), which may facilitate their recovery from large bodies of water.

3.3. Metal Ion Adsorption. The adsorption capacity of the EDTA-inspired polydentate hydrogel was determined by immersing it in a solution of various kinds of metal ions (hard-Cr^{3+}; borderline-Zn^{2+}, Cu^{2+}, and Pb^{2+}; and soft-Hg^{2+} and Cd^{2+}) that are commonly found in polluted water. HG-1 gel was chosen for this study because of its high swelling ratio (5846%) and considerable mechanical strength (G' = 341 Pa).

The metal ion adsorption isotherm of the hydrogel was determined with increasing concentrations (5−500 ppm) of three different metal ions, Cr^{3+} (hard acid), Cu^{2+} (borderline acid), and Hg^{2+} (soft acid). The adsorption isotherm (Figure S4a) demonstrated an increasing order of adsorption capacity up to 50 ppm followed by gradual reaching of adsorption equilibrium with increasing concentrations of metal ion. The experimental data were fitted with the Langmuir isotherm (Figure S4b) and the Freundlich isotherm (Figure S4c). The linear correlation coefficients for the metal ions Cr^{3+}, Cu^{2+}, and Hg^{2+} were 0.997, 0.994, and 0.995, as obtained from the Langmuir isotherm, and 0.813, 0.833, and 0.844, as obtained from the Freundlich isotherm, respectively. The correlation coefficients near 1 revealed that the hydrogels followed the Langmuir adsorption isotherm indicating the monolayer adsorption of metal ions, which also corroborated well with the earlier report.[6] Various calculated parameters corresponding to the Langmuir and Freundlich adsorption isotherms are presented in Table S1.

The maximum adsorption capacity of the hydrogel for different metal ions (single-component system, Figure 4a), Zn^{2+}, Cu^{2+}, Pb^{2+}, Cr^{3+}, Hg^{2+}, and Cd^{2+}, were determined as 439.3, 436.5, 395.1, 340.6, 285.1, and 210.7 mg/g, respectively. The hydrogel showed a relatively high adsorption capacity for the borderline metal ions Zn^{2+}, Cu^{2+}, and Pb^{2+} than either of the hard (Cr^{3+}) or soft (Hg^{2+} and Cd^{2+}) metal ions. The results also revealed the nonspecific adsorption behavior of the hydrogel, which is essential for the removal of a broad range of heavy metal pollutants. Most importantly, the observed metal ion adsorption capacities of this hydrogel were significantly higher than the reported values for similar types of hydrogels (Table 2). The higher adsorption capacity for metal ions was attributed to the porous three-dimensional structure of the hydrogel with numerous metal-coordinating functional groups (−COOH, $-NH_2$, $-NR_2$, and $-NR_3$) as displayed in Scheme 1. Note that the literature-reported theoretical adsorption capacity[9] (592 mg/g for Hg, Table 2) of the EDTA-modified MOF is higher than our hydrogel. However, these theoretical data were obtained after fitting with the Langmuir isotherm, not from the actual experiment.

To mimic the environment of polluted water, the hydrogel HG-1 was immersed in a mixture of six metal ions (50 ppm each), and the average adsorption capacity for each metal ion in the multiple-component system was determined to be 90.98 (Zn^{2+}), 94.81 (Cu^{2+}), 86.41 (Pb^{2+}), 89.12 (Cr^{3+}), 82.33 (Hg^{2+}), and 34.57 (Cd^{2+}) mg/g (Figure 4b). The total adsorption capacity of the hydrogel from the multiple-component system (i.e. the sum of all the six metal ions adsorbed from the mixture of ions) was 482.2 mg/g, which was higher than the maximally adsorbed Zn^{2+} and Cu^{2+} ions from the single-component system (Figure 4a).

Table 2. Summary of Adsorption Capacity Reported in the Literature in Comparison with Our Current EDTA-Inspired Polydentate Hydrogel (HG-1)

adsorbents	metal ions	adsorption capacity (mg/g)	reference
EDTA-inspired polydentate hydrogel from HPAM and BPEI	Zn^{2+}	439.3	this study
	Cu^{2+}	436.5	
	Pb^{2+}	395.1	
	Cr^{3+}	340.6	
	Hg^{2+}	285.1	
	Cd^{2+}	210.7	
EDTA cross-linked polyacrylamide hydrogel	Cu^{2+}	99.4	5
	Pb^{2+}	138.4	
	Cd^{2+}	86.0	
cellulose nanocrystals and graphene quantum dot-based hydrogel	Cu^{2+}	230.0	29
	Hg^{2+}	115.0	
	Ni^{2+}	110.0	
	Ag^{+}	160.0	
EDTA-grafted covalent organic framework	$Cr3^{+}$	53.0	16
	Cu^{2+}	58.0	
	Pd^{2+}	65.0	
EDTA-modified chitosan−silica hybrid material	Pb^{2+}	166.3	30
	Cd^{2+}	141.4	
EDTA-functionalized magnetic chitosan	Cu^{2+}	151.1	18
	Pb^{2+}	189.3	
EDTA-modified MOFs	La^{3+}	205.0[a]	9
	Hg^{2+}	592.0[a]	
	Pb^{2+}	313.0[a]	

[a]Theoretically obtained adsorption capacity after fitting with the Langmuir adsorption isotherm.

The single-component adsorption results indicate that the adsorption capacities of metal ions follow the order: $Cu^{2+} \simeq Zn^{2+} \simeq Pb^{2+} > Cr^{3+} > Hg^{2+} > Cd^{2+}$. The results of the multiple-component adsorption study, where competition is expected, show the following order: $Cu^{2+} \simeq Zn^{2+} \simeq Pb^{2+} \simeq Cr^{3+} \simeq Hg^{2+} > Cd^{2+}$. Based on these observations, three points are made. First, borderline metals ions (Cu^{2+}, Zn^{2+}, and Pb^{2+}) tend to be more highly adsorbed by our hydrogels than either hard or soft metal ions. Second, the increased adsorption level of Cr^{3+} and Hg^{2+} in the multiple-component system suggests that these two metal ions may have competitive advantages over other metal ions. It is known that Cr^{3+} and Hg^{2+} form more stable complexes with EDTA (log K_f = 23.4 and 21.5, respectively) than other ions.[28] A similar explanation may apply to Cr^{3+}/Hg^{2+}−hydrogel complexes. Third, Cd^{2+} is the least competitive among all the ions tested. This observation is consistent with numerous literature reports on EDTA-functionalized materials (Table 2).

To determine the kinetics of adsorption, 50 mL of each metal ion solution (50 ppm) was separately incubated with the hydrogel HG-1 at 0.1 mg/mL, and the adsorption capacity was measured at various time points (Figure S5a). The kinetics showed initial fast adsorption of metal ions, indicating a strong

https://dx.doi.org/10.1021/acsami.0c03689
ACS Appl. Mater. Interfaces 2020, 12, 25276−25285

interaction between the hydrogel and the metal ion, followed by the gradual approach to equilibrium. The ratio of adsorption time (t) and adsorption capacity at time t (q_t), "t/q_t", highly linearly correlated with time, "t" (linear correlation coefficient R^2 = 0.99, Figure S5b), revealing that the adsorption process followed pseudo-second-order kinetics (eq 2) and was chemisorptive in nature, which served as the rate-controlling step.[9] Various calculated parameters corresponding to the pseudo-first-order (Figure S5c) and pseudo-second-order kinetic models (Figure S5b) are presented in Table S2.

The reusability of the adsorbent is one of the challenging tasks to reduce the cost of wastewater treatment. Adsorbents can be reused if they possess the following characteristics: (a) enough mechanical integrity to be recollected from the waterbodies after adsorption and (b) capability to reproduce enough adsorption sites during the regeneration process to adsorb newly introduced metal ions. The higher mechanical integrity of the hydrogel had already been observed from their high storage modulus, which was accompanied by its self-healing capacity. Furthermore, the regeneration of the hydrogel was tested with three highly adsorbed metal ions, Cu^{2+}, Zn^{2+}, and Pb^{2+}. After each cycle of metal ion adsorption, the hydrogel was regenerated by immersing in a 5% HNO_3 solution for 24 h followed by separation and washing with Milli-Q water. After the 1st cycle of regeneration, the hydrogel retained about 91.6, 93.1, and 87.7% of adsorption efficiency for Cu^{2+}, Zn^{2+}, and Pb^{2+}, respectively (Figure 5). Even after

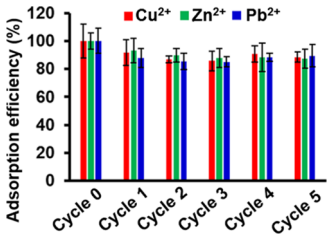

Figure 5. Adsorption efficiency of the polydentate hydrogel for three metal ions preserved after at least five cycles of adsorption−regeneration.

five cycles of regeneration, the adsorption capacity of the hydrogel was still 88.5, 87.1, and 89.3% for Cu^{2+}, Zn^{2+}, and Pb^{2+}, respectively. The excellent reusability of the hydrogel even after five cycles of regeneration proves that our hydrogel is a highly cost-effective adsorbent for heavy metals.

Polluted water may contain certain inorganic ions such as Ca^{2+}, Mg^{2+}, Na^+, and K^+. Studies have shown that the stability of the EDTA−metal ion complex mostly follows this trend: heavy metal ions > Ca^{2+} > Mg^{2+} >Na^+ > K^+.[5] For metal-scavenging polymers similar to EDTA, it is thus reasonable to expect that the adsorbed heavy metal ions may not be displaced easily by other ions. It is possible in some circumstances that nonheavy metal ions could compete with heavy metals and reduce the heavy metal adsorption capacity of the materials to some extent. However, the effect will depend on the amount of nonheavy metal ions present relative to that of heavy metal ions, which are usually more abundant in polluted water. Furthermore, natural organic matter (NOM) is a broad class of organic materials existing in polluted water with various metal ion binding capacities. The presence of NOM could reduce the adsorption capacity of hydrogels; however, it is also subject to the percentage and types of NOM present in polluted water.[31]

3.4. Adsorption Mechanism. The underlying mechanism of metal ion adsorption by the EDTA-inspired polydentate hydrogel was investigated by XPS analysis of the metal ion-adsorbed hydrogel. The O 1s HR-XPS spectrum of the Cu^{2+} ion-adsorbed hydrogel showed peaks at 528.8 and 530.2 eV, which were assigned to "$-CONH_2$" and "−COOH", respectively (Figure 1h). A peak at a higher binding energy (531.5 eV) appeared only in the Cu^{2+}-adsorbed gel but not in the gel without a metal ion (comparing Figure 1h with Figure 1d). This signal was attributed to the significant coordinate bonding interaction between the "−COOH" group of the hydrogel and the Cu^{2+} ion. Furthermore, the N 1s spectrum of the hydrogel showed peaks at 397.2 and 399.3 eV, which were assigned to "$-CONH_2$" and "−CONH(BPEI)", respectively. The shifting of the N 1s binding energy peak corresponding to "−CONH(BPEI)" from 398.6 (for the hydrogel without ions, Figure 1f) to 399.3 eV (Figure 1g) confirmed the engagement of the "−NH−" group of BPEI in coordination with the Cu^{2+} ions. Furthermore, the change in hydrogel's color from light yellow to blue (Figure S3d) after adsorption of the Cu^{2+} ion revealed that ion adsorption was because of the formation of coordination complexes. Along with coordination, it is possible that additional mechanisms such as electrostatic interaction and ion exchange may also play a role.

Because metal ion adsorption by our EDTA-inspired polydentate hydrogels is mechanistically similar to other EDTA-modified adsorbents reported in the literature,[18] we expect that the adsorption process would result in a negative ΔG value and be spontaneous. In addition, the adsorption is likely exothermic ($\Delta H < 0$) with a decrease of molecular randomness ($\Delta S < 0$) at the hydrogel/metal ion solution interface.

3.5. Biocompatibility. The biocompatibility of the EDTA-inspired polydentate hydrogel was assessed by measuring cytotoxicity in mouse NIH/3T3 fibroblasts treated with 50, 100, 500, and 1000 μg/mL of the dry hydrogel for 24 h. The results (Figure S6a) showed more than 80% cell viability even at the highest dosage of hydrogel (1000 μg/mL). Hence, this hydrogel shows high biocompatibility and safety to human cells. Furthermore, the cells were cultured with the hydrogel at 1000 μg/mL for 24 h, and the cell morphology was examined by fluorescence microscopy. A piece of the hydrogel can be clearly seen in the microscopic image (Figure S6b). The transparency of the hydrogel allowed us to capture clear microscopic images of the cells even in the presence of hydrogel. After comparing the hydrogel-treated cells with the control experiment, one can effortlessly notice that the hydrogel has no negative impact on cell growth. Hence, this experiment further supports the biocompatibility nature of our hydrogel, revealing the absence of any associated secondary pollution.

4. CONCLUSIONS

We have successfully synthesized EDTA-inspired polydentate hydrogels using the cost-effective synthetic polymer HPAM and the short-chain BPEI as a multifunctional cross-linker. The hydrogels (visualized by SEM) revealed a reduction in the average pore size from 70 to 30 μm with increasing nominal wt % of the cross-linker from 10 wt % to 20 wt %. These hydrogels with a large number of EDTA-inspired metal-chelating groups (−COOH, $-NR_2$, and −NHR) displayed a

https://dx.doi.org/10.1021/acsami.0c03689
ACS Appl. Mater. Interfaces 2020, 12, 25276−25285

maximum adsorption capacity of 482.2 mg/g (for multicomponent system), higher than any earlier reports of metal-binding materials. Furthermore, the hydrogels displayed a broad spectrum adsorption capacity of 439.3, 436.5, 395.1, 340.6, 285.1, and 210.7 mg/g for Zn^{2+}, Cu^{2+}, Pb^{2+}, Cr^{3+}, Hg^{2+}, and Cd^{2+}, respectively. The hydrogel demonstrated self-healing property and showed a retention of adsorption capacity of >85% even after the 5th cycle of its reuse. Furthermore, cytocompatibility of the hydrogel was demonstrated by its high cell viability (>80%) at dosages as high as 1 mg/mL. Therefore, the EDTA-inspired polydentate hydrogels combine exceptionally high nonspecific adsorption capacity with high biocompatibility, mechanical strength, self-healing ability, and reusability. They are cost-effective materials for removing a broad spectrum of heavy metal ions from polluted water systems.

■ ASSOCIATED CONTENT

Supporting Information

The Supporting Information is available free of charge at https://pubs.acs.org/doi/10.1021/acsami.0c03689.

NMR and FTIR spectra of polymer precursors and hydrogels, images of the dry and swollen hydrogel, demonstration of hydrogel self-healing, change in the adsorption capacity of the hydrogel with adsorption time and with equilibrium concentration of the metal ion, and calculated parameters of the kinetic models and the adsorption models (PDF)

■ AUTHOR INFORMATION

Corresponding Authors

Sudipta Panja − *Department of Biomedical Engineering, University of Minnesota, Minneapolis, Minnesota 55455, United States; McKetta Department of Chemical Engineering, University of Texas at Austin, Austin, Texas 78712, United States;* orcid.org/0000-0001-5692-450X; Phone: +1-512-576-2995; Email: spanja@umn.edu, sudiptapanjachem@gmail.com

Chun Wang − *Department of Biomedical Engineering, University of Minnesota, Minneapolis, Minnesota 55455, United States;* orcid.org/0000-0003-2634-4795; Phone: +1-612-626-3990; Email: wangx504@umn.edu

Author

Samuel Hanson − *Department of Biomedical Engineering, University of Minnesota, Minneapolis, Minnesota 55455, United States*

Complete contact information is available at: https://pubs.acs.org/10.1021/acsami.0c03689

Notes

The authors declare no competing financial interest.

■ ACKNOWLEDGMENTS

S.P. acknowledges IPRIME, University of Minnesota, Twin Cities, USA, and National Science Foundation through the Center for Dynamics and Control of Materials: an NSF MRSEC under Cooperative agreement no. DMR-1720595 at University of Texas at Austin for funding. The authors appreciate the generous support and advice of Prof. Nathaniel A. Lynd (University of Texas—Austin) and Prof. Ron Siegel (University of Minnesota).

■ REFERENCES

(1) Mohammed, N.; Baidya, A.; Murugesan, V.; Kumar, A. A.; Ganayee, M. A.; Mohanty, J. S.; Tam, K. C.; Pradeep, T. Diffusion-Controlled Simultaneous Sensing and Scavenging of Heavy Metal Ions in Water Using Atomically Precise Cluster−Cellulose Nanocrystal Composites. *ACS Sustainable Chem. Eng.* **2016**, *4*, 6167−6176.

(2) WHO. Diarrhoeal Disease. https://www.who.int/en/news-room/fact-sheets/detail/diarrhoeal-disease, 2017.

(3) Zou, Y.; Wang, X.; Khan, A.; Wang, P.; Liu, Y.; Alsaedi, A.; Hayat, T.; Wang, X. Environmental Remediation and Application of Nanoscale Zero-Valent Iron and Its Composites for the Removal of Heavy Metal Ions: A Review. *Environ. Sci. Technol.* **2016**, *50*, 7290−7304.

(4) Wen, T.; Wu, X.; Tan, X.; Wang, X.; Xu, A. One-pot Synthesis of Water-swellable Mg-Al Layered Double Hydroxides and Graphene Oxide Nanocomposites for Efficient Removal of As(V) from Aqueous Solutions. *ACS Appl. Mater. Interfaces* **2013**, *5*, 3304−3311.

(5) Ma, J.; Zhou, G.; Chu, L.; Liu, Y.; Liu, C.; Luo, S.; Wei, Y. Efficient Removal of Heavy Metal Ions with An EDTA Functionalized Chitosan/Polyacrylamide Double Network Hydrogel. *ACS Sustainable Chem. Eng.* **2016**, *5*, 843−851.

(6) Li, B.; Zhang, Y.; Ma, D.; Shi, Z.; Ma, S. Mercury Nano-trap for Effective and Efficient Removal of Mercury(II) from Aqueous Solution. *Nat. Commun.* **2014**, *5*, 5537.

(7) Ding, S.-Y.; Dong, M.; Wang, Y.-W.; Chen, Y.-T.; Wang, H.-Z.; Su, C.-Y.; Wang, W. Thioether-Based Fluorescent Covalent Organic Framework for Selective Detection and Facile Removal of Mercury-(II). *J. Am. Chem. Soc.* **2016**, *138*, 3031−3037.

(8) Sun, Q.; Aguila, B.; Perman, J.; Earl, L. D.; Abney, C. W.; Cheng, Y.; Wei, H.; Nguyen, N.; Wojtas, L.; Ma, S. Postsynthetically Modified Covalent Organic Frameworks for Efficient and Effective Mercury Removal. *J. Am. Chem. Soc.* **2017**, *139*, 2786−2793.

(9) Peng, Y.; Huang, H.; Zhang, Y.; Kang, C.; Chen, S.; Song, L.; Liu, D.; Zhong, C. A Versatile MOF-based Trap for Heavy Metal Ion Capture and Dispersion. *Nat. Commun.* **2018**, *9*, 187.

(10) Panja, S.; Dey, G.; Bharti, R.; Mandal, P.; Mandal, M.; Chattopadhyay, S. Metal Ion Ornamented Ultrafast Light-Sensitive Nanogel for Potential in Vivo Cancer Therapy. *Chem. Mater.* **2016**, *28*, 8598−8610.

(11) Wang, L.-Y.; Wang, M.-J. Removal of Heavy Metal Ions by Poly(vinyl alcohol) and Carboxymethyl Cellulose Composite Hydrogels Prepared by a Freeze−Thaw Method. *ACS Sustainable Chem. Eng.* **2016**, *4*, 2830−2837.

(12) Sun, S.; Wang, L.; Wang, A. Adsorption Properties of Crosslinked Carboxymethyl-chitosan Resin with Pb(II) as Template Ions. *J. Hazard Mater.* **2006**, *136*, 930−937.

(13) Godiya, C. B.; Li, D.; Chen, Z.; Lu, X. Carboxymethyl Cellulose/Polyacrylamide Composite Hydrogel for Cascaded Treatment/Reuse of Heavy Metal Ions in Wastewater. *J. Hazard. Mater.* **2019**, *364*, 28−38.

(14) Prathap, A.; Raju, C.; Sureshan, K. M. Organogel-Derived Covalent-Noncovalent Hybrid Polymers as Alkali Metal-Ion Scavengers for Partial Deionization of Water. *ACS Appl. Mater. Interfaces* **2018**, *10*, 15183−15188.

(15) El-Hamshary, H.; El-Garawany, M.; Assubaie, F. N.; Al-Eed, M. Synthesis of Poly(acrylamide-co-4-vinylpyridine) Hydrogels and Their Application in Heavy Metal Removal. *J. Appl. Polym. Sci.* **2003**, *89*, 2522−2526.

(16) Jiang, Y.; Liu, C.; Huang, A. EDTA-Functionalized Covalent Organic Framework for the Removal of Heavy-Metal Ions. *ACS Appl. Mater. Interfaces* **2019**, *11*, 32186−32191.

(17) Cheng, R.; Zhuang, S.; Shi, L.; Zheng, X.; Wang, J. Adsorption of Sr(II) from Water by Mercerized Bacterial Cellulose Membrane Modified with EDTA. *J. Hazard Mater.* **2019**, *364*, 28−38.

(18) Chen, B.; Zhao, H.; Chen, S.; Long, F.; Huang, B.; Yang, B.; Pan, X. A Magnetically Recyclable Chitosan Composite Asorbent Functionalized with EDTA for Simultaneous Capture of Anionic Dye and Heavy Metals in Complex Wastewater. *Chem. Eng. J.* **2019**, *356*, 69−80.

(19) Cordova, M.; Cheng, M.; Trejo, J.; Johnson, S. J.; Willhite, G. P.; Liang, J.-T.; Berkland, C. Delayed HPAM Gelation via Transient Sequestration of Chromium in Polyelectrolyte Complex Nanoparticles. *Macromolecules* **2008**, *41*, 4398−4404.
(20) Bai, Y.; Xiong, C.; Wei, F.; Li, J.; Shu, Y.; Liu, D. Gelation Study on a Hydrophobically Associating Polymer/Polyethylenimine Gel System for Water Shut-off Treatment. *Energy Fuels* **2015**, *29*, 447−458.
(21) Hoerter, J. M.; Gellman, S. H.; Cui, Q.; Stahl, S. S. Discovery and Mechanistic Study of AlIII-Catalyzed Transamidation of Tertiary Amides. *J. Am. Chem. Soc.* **2008**, *130*, 647−654.
(22) Cheung, C. W.; Ma, J.-A.; Hu, X. Manganese-Mediated Reductive Transamidation of Tertiary Amides with Nitroarenes. *J. Am. Chem. Soc.* **2018**, *140*, 6789−6792.
(23) Zeynali, M. E.; Rabiei, A. Alkaline Hydrolysis of Polyacrylamide and Study on Poly(acrylamide-co-sodium acrylate) Properties. *Iran. Polym. J.* **2002**, *1*, 269−275.
(24) Lai, J.; Xu, Z.; Tang, R.; Ji, W.; Wang, R.; Wang, J.; Wang, C. PEGylated Block Copolymers Containing Tertiary Amine Side-chainscleavable via Acid-labile Ortho Ester Linkages for pH-Triggered Release of DNA. *Polymer* **2014**, *55*, 2761−2771.
(25) Hsiao, M.-H.; Lin, K.-H.; Liu, D.-M. Improved pH-responsive Amphiphilic Carboxymethyl-hexanoyl chitosan−poly(acrylic acid) Macromolecules for Biomedical Applications. *Soft Matter* **2013**, *9*, 2458−2466.
(26) Lu, Y.; Zhao, Z.; Bi, L.; Chen, Y.; Wang, J.; Xu, S. Synthesis of a Multifunctional Hard Monomer from Rosin: the relationship of allyl structure in maleopimarate and UV-curing property. *Sci. Rep.* **2018**, *8*, 2399.
(27) Melnyk, O.; Agouridas, V. From Protein Total Synthesis to Peptide Transamidation and Metathesis: playing with the reversibility of N,S-acyl or N,Se-acyl migration reactions. *Curr. Opin. Chem. Biol.* **2014**, *22*, 137−145.
(28) Harris, D. C. *Quantitative Chemical Analysis*, 9th ed.; W. H. Freeman and Company, 2016.
(29) Alizadehgiashi, M.; Khuu, N.; Khabibullin, A.; Henry, A.; Tebbe, M.; Suzuki, T.; Kumacheva, E. Nanocolloidal Hydrogel for Heavy Metal Scavenging. *ACS Nano* **2018**, *12*, 8160−8168.
(30) Zhao, F.; Repo, E.; Yin, D.; Chen, L.; Kalliola, S.; Tang, J.; Iakovleva, E.; Tam, K. C.; Sillanpää, M. One-pot Synthesis of Trifunctional Chitosan-EDTA-beta-cyclodextrin Polymer for Simultaneous Removal of Metals and Organic Micropollutants. *Sci. Rep.* **2017**, *7*, 15811.
(31) Schmitt, D.; Taylor, H. E.; Aiken, G. R.; Roth, D. A.; Frimmel, F. H. Influence of Natural Organic Matter on the Adsorption of Metal Ions onto Clay Minerals. *Environ. Sci. Technol.* **2002**, *36*, 2932−2938.

https://dx.doi.org/10.1021/acsami.0c03689
ACS Appl. Mater. Interfaces 2020, 12, 25276−25285